Colloid Polym Sci (2008) 286:1193–1202
DOI 10.1007/s00396-008-1889-8

ORIGINAL CONTRIBUTION

Crystallization behavior and hydrophilicity of poly (vinylidene fluoride) (PVDF)/poly (styrene-*co*-acrylonitrile) (SAN) blends

Wenzhong Ma · Jun Zhang · Shuangjun Chen · Xiaolin Wang

Received: 12 April 2008 / Revised: 8 May 2008 / Accepted: 9 May 2008 / Published online: 8 June 2008

Abstract Poly (styrene-*co*-acrylonitrile) (SAN) is a hydrophilic non-crystalline copolymer, which is initially used in this paper to improve the hydrophilicity of poly (vinylidene fluoride) (PVDF). Investigation of the crystallization behavior of PVDF/SAN blends showed that the samples presented only α phase regardless of SAN content as cooling from the melt. A double-melting phenomenon was related to the perfection or crystal size of PVDF crystals. As the SAN content is increasing, crystallization of PVDF was limited, leading to a decreased crystallinity and lamellar growth. Besides, the hydrophilicity of PVDF was improved by blending with SAN. The sample containing 70 wt.% SAN performed a similar surface property of the neat SAN owing to the besieging of the PVDF phase by SAN. Observed from the cross section of the blends, PVDF/SAN blends were partially miscible with less than 50 wt.% SAN addition. As the SAN content was more than 50 wt.%, the crystalline PVDF particles clearly dispersed in the amorphous matrix.

Keywords Crystallization · Blends · Hydrophilicity · Poly (vinylidene) fluoride (PVDF)

W. Ma · J. Zhang (✉) · S. Chen
College of Materials Science and Engineering,
Nanjing University of Technology,
Nanjing 210009, China
e-mail: zhangjun@njut.edu.cn

X. Wang
Department of Chemical Engineering,
Tsinghua University,
Beijing 100084, China

Introduction

Poly (vinylidene) fluoride (PVDF), as a semi-crystalline polymer with a very low T_g (−40 °C), has wide applications due to its excellent physical and chemical properties, as well as good thermal stability [1]. So, it is quite flexible and suitable for membrane application in temperature ranging between −50 °C and 140 °C, just prior to its melting temperature [2–5]. However, because of the hydrophobic nature of the PVDF, its membranes often suffer from low flux, changing the solute selectivity with time, and surface fouling, during filtration of oil/protein containing solutions. Thus, a number of efforts have been devoted to the chemical and physical modification of PVDF to improve its surface hydrophilicity.

Surface functionalization of a polymer is one of the traditional and effective processes to improve its hydrophilicity, including chemical treatment [6], irradiation [7, 8], plasma treatment [9], and ozone treatment [10]. It is then demonstrated that through the intelligent choice of the hydrophilic molecular functionality of the graft chains, the molecules of PVDF surface can be redesigned to impart hydrophilicity to its surface. Indeed, these techniques affect the chemical nature of the membrane surface layer without altering that of the sub-layer support. But it is easily removed and likely to be accompanied by changes in membrane pore size and pore size distribution, leading to reduced permeability [11]. Thus, alternative approach is based on molecular or bulk graft copolymerization [12, 13], by which the pore surfaces is dependent on the copolymer structure and composition. This method is complicated, and the process should add substantial costs.

Blending, as a versatile, straightforward, and relatively inexpensive method for modifying the properties of

polymer materials, has attracted tremendous attention over the past decades because of the large improvements exhibiting the properties of all the constituent components for special applications. From an exclusively thermodynamic point of view, the blends may be classified as miscible, partially miscible, and immiscible [14]. PVDF/poly (methyl methacrylate) (PMMA) is a miscible system [15–17], which is linked to the existence of a single phase and to property isotropy. The hydrophilic membranes of PVDF/PMMA blends were prepared, and the hydrophilicity was enhanced and flux rate of the membrane increased by PMMA addition [18, 19]. PVDF/poly (vinylpyrrolidone) is also a miscible blend, and the existence of crystallized phase at the surface would affect the surface hydrophilicity [20]. In Hester and coworkers' publications [21, 22], the blends of PVDF and a free-radically synthesized amphiphilic comb polymer significantly enhanced fouling resistance and the provided hydrophilic surfaces with excellent stability. With regard to a partially miscible system, the hydrophilicity of PVDF can be enhanced by adding hydrophilic polyacrilonitrile (PAN) [23, 24]. The immiscible system has fewer applications owing to the gross phase separation and poor interfacial adhesion [25]. So, selecting a suitable polymer, which is hydrophilic to blend with PVDF, is the key factor. The copolymer of styrene and acrylonitrile (SAN) is a hydrophilic polymer because of the acrylonitrile units in this copolymer [26]. However, few works focused on the hydrophilicity of PVDF/SAN system. In the similar work, Yang's group [23, 26] has investigated PAN/PVDF blend membranes but did not clarify the relationship between the PAN addition and the crystallization of PVDF and did not give out the surface tension of the blend samples.

Furthermore, PVDF has four of the PVDF crystalline phases that exist, so-called α, β, γ, and δ [27, 28], according to the conformation of the chains and their molecular packing at different temperatures [29, 30]. In the blends, the crystalline phase of PVDF depended on the PMMA content in the blends [31, 32]. In our previous work, the crystallization of PVDF is affected by the diluents during the thermally induced phase separation [4], by the mixed solvent, and by substrates in the solution casting process [33, 34]. PVDF/PMMA blends, which are prepared by solution casting, can improve the hydrophilicity of PVDF efficiently [35]; however, the solvent residue in the samples was hard to remove completely.

The present work dealt with the crystallization behaviors and hydrophilicity of PVDF by melt blending with SAN. The hydrophilicity of PVDF blending with SAN under different polymer ratios was investigated. Simultaneously, the crystallization behavior of PVDF with different composition of SAN addition was discussed.

Experimental

Materials

PVDF (Kynar K-761, $\overline{\mathrm{M}}\mathrm{w} = 441,000$) was supplied by Elf Atochem of North America Inc. (USA). SAN (D-178, in which the acrylonitrile content is 26 wt.%) was purchased from Zhenjiang Guoheng Chemical Limited Company (China).

Melt blending and specimen preparation

The melt blending of PVDF/SAN was carried out with a torque rheogoniometer (Kechuang machinery XSS-300) at 180 °C and 60 rpm for 10 min. A set of the blends with weight fractions of PVDF containing 100%, 90%, 70%, 50%, 30%, 10%, and 0% (*w*/*w*) were prepared. Then, the blend samples were prepared by compression molding at 180 °C with the platen vulcanizing press for 10 min. Subsequently, they were cooled freely on another cold platen vulcanizing press at room temperature. Thus, the flat sheet samples (about 0.5 mm) possessing smooth surfaces were obtained, which denoted as the melt-crystallized samples. Subsequently, the series of measurements were performed.

Characterization techniques

Fourier transform infrared spectroscopy (FTIR) spectra were obtained by a Bruker IFS-66/s with 4-cm^{-1} resolution. FTIR-attenuated total reflection (ATR) spectra were applied in this work.

Wide angle X-ray diffraction (WAXD) was done in a Shimadzu XRD-6000 diffractometer (Cu K_α radiation, 40 kV and 30 mA). The scanning angle ranged from 5° to 50° with the scanning velocity of 4°/min.

Differential scanning calorimetry (DSC) was conducted using a Perkin-Elmer DSC-7C thermal analysis apparatus. For the sample measurement, about 10 mg of each sample was sealed into an aluminum pan. Then, the melting tests were run at a heating rate of 10 °C/min from 25 °C to 180 °C under a dry argon blanket. The crystallization process of the blends was detected by holding the samples in DSC at 180 °C for 10 min followed by cooling at a controlled rate of 5 °C/min. The crystallinity X_c was evaluated as in our previous work [35]. The crystallization half time ($t_{1/2}$), which is defined as the half time of crystallization [36], was used as a characteristic parameter of the crystallization process.

Scanning electron microscopy (SEM) micrographs of the cross sections of various blends coating with gold were taken with a Jeol JSM-5900 instrument. Before the observation, the samples were fractured in liquid nitrogen, and the fractured surfaces were obtained.

The measurement of the contact angle of samples was carried out using a Krüss DSA-100 goniometer at 20 °C. Water and diiodomethane were used as the test liquids. The detailed procedure was the same as our previous work [35]. Then, the total solid surface tension γ_s, and its dispersive and polar component γ_s^d, γ_s^p were calculated by Owens and Wendt method [37, 38].

Results and discussion

The miscibility of SAN with PVDF

According to the miscibility of solvents and polymers [39], for a system with (a) no volume change on mixing at constant pressure, (b) no reaction between the components, and (c) no complex formation or special associations, the miscibility of two polymers is mainly governed by the solubility parameter (δ) of two polymers. Applying to a polyblend system, the closer the value of δ is for each component, the easier it is for them to mix homogeneously. As reported, the solubility parameter values of PVDF and SAN is 19.2 and 20.4 $(J/cm^3)^{1/2}$, respectively (the latter one calculated by group contributions) [39]. The absolute value of their difference is more than 1.0 $(J/cm^3)^{1/2}$, making PVDF/SAN blends not entirely miscible actually, according to the literature [24]. The SEM observation of the cross section is a qualitative way to confirm the phase morphology of this polyblends. Figure 1 shows the microscopic investigation of the cross section of the blends with various mass ratios of each component. It is clearly shown that the neat PVDF and SAN samples have only one homogeneous phase (Fig. 1a,g), but two phases of this two polymers can be observed in their blends. In SAN-rich phase (SAN≥50 wt. %), the crystalline PVDF particle clearly disperses in the SAN and PVDF amorphous matrix, and the size of crystalline PVDF particle decreases with the further increase of SAN content (Fig. 1d–f). In contrast, in PVDF-rich phase (SAN<50 wt.%), the boundary of this two polymer is obscure because the amorphous region of PVDF and SAN can be formed as a continuous morphology. Compared with the immiscible PVDF/polycarbonate system [25] in which one phase disperses in the co-continuous phase with a change of each component and the obvious interspace between the two polymers can be clearly seen, PVDF/SAN system can be attributed to the partially miscible to a great extent. As the SAN content is more than 50 wt.%, the PVDF/SAN blends are the immiscible systems, whereas the blends with the SAN content <50 wt.%, the systems can be considered as the partially miscible ones.

FTIR spectroscopy

The IR spectroscopy in ATR mode is employed to characterize the PVDF crystalline phases in the melt-crystallized blends. As shown in Fig. 2, the PVDF blends with different weight fraction of SAN, melted and subsequently cooled at room temperature, have the well-defined absorption bands at 1,423, 1,400, 1,383, 1,210, 1,177, 1,068, 975, 870, 855, 794, 761, and 614 cm^{-1}. As reported, the absorption bands at 1,400, 1,068, and 870 cm^{-1} are common to forms α, β, and γ, but bands at 1,423, 1,383, 1,210, 1,177, 975, 855, 794, 761, and 614 cm^{-1} represent the characteristic spectrum of the α phase of PVDF crystal [30, 40]. It indicates that the only crystallization of α phase PVDF predominates in the crystallization from the melt, which agrees with Gregorio's results [32]. It can be seen that the increase in SAN addition results in a decrease in intensity of the characteristic α phase bands. This suggests that the crystallization of PVDF is reduced by SAN addition. As the SAN content is half in the blend, the band at 761 cm^{-1} shifts to the lower wave number. This can be attributed to the overlapping of the out-of-plane hydrogen vibration of SAN (at 759 cm^{-1}) [41] and the α phase band of PVDF (at 761 cm^{-1}). As the SAN content increases in the blend, this overlapped band becomes broader owing to the domination of SAN. The band at 699 cm^{-1}, which also represents the out-of-plane hydrogen vibration of SAN [41], becomes more obvious as SAN content increased.

WAXD analysis

In order to confirm the crystalline phase in the melt-crystallized blends, X-ray diffractometry is applied, as shown in Fig. 3. According to the researchers' work [29, 30, 42], the peaks at 2θ=18.05°, 18.70°, 20.27°, 25.93°, 26.90°, 33.37°, 36.17°, 37.43°, and 39.00° in the curve for the neat PVDF sample (Fig. 3a) represent the diffractions in planes (100), (020), (110), (120), (021), (130), (200), (210), and (002), respectively, which are all characteristic of the α phase of PVDF. It is verified that all samples by melt molding, despite the various SAN weight fraction in the blend, presents predominantly the α phase. Among these peaks, three strong ones at 2θ=18.05°, 18.70°, and 20.27° have a decrease in their intensity, as the SAN composition increased in the blend. Especially for the one at 2θ=18.70°, the decrease in a change is the most remarkable. The intensity of other weak peaks at high degree (25°~40°) is also decreased with the SAN incorporation. As demonstrated, the crystallinity of a crystalline polymer can be related to the total scattering height of the peak in the WAXD [43]. Therefore, the crystallinity of PVDF in the blends is affected by the increased SAN content. As the weight

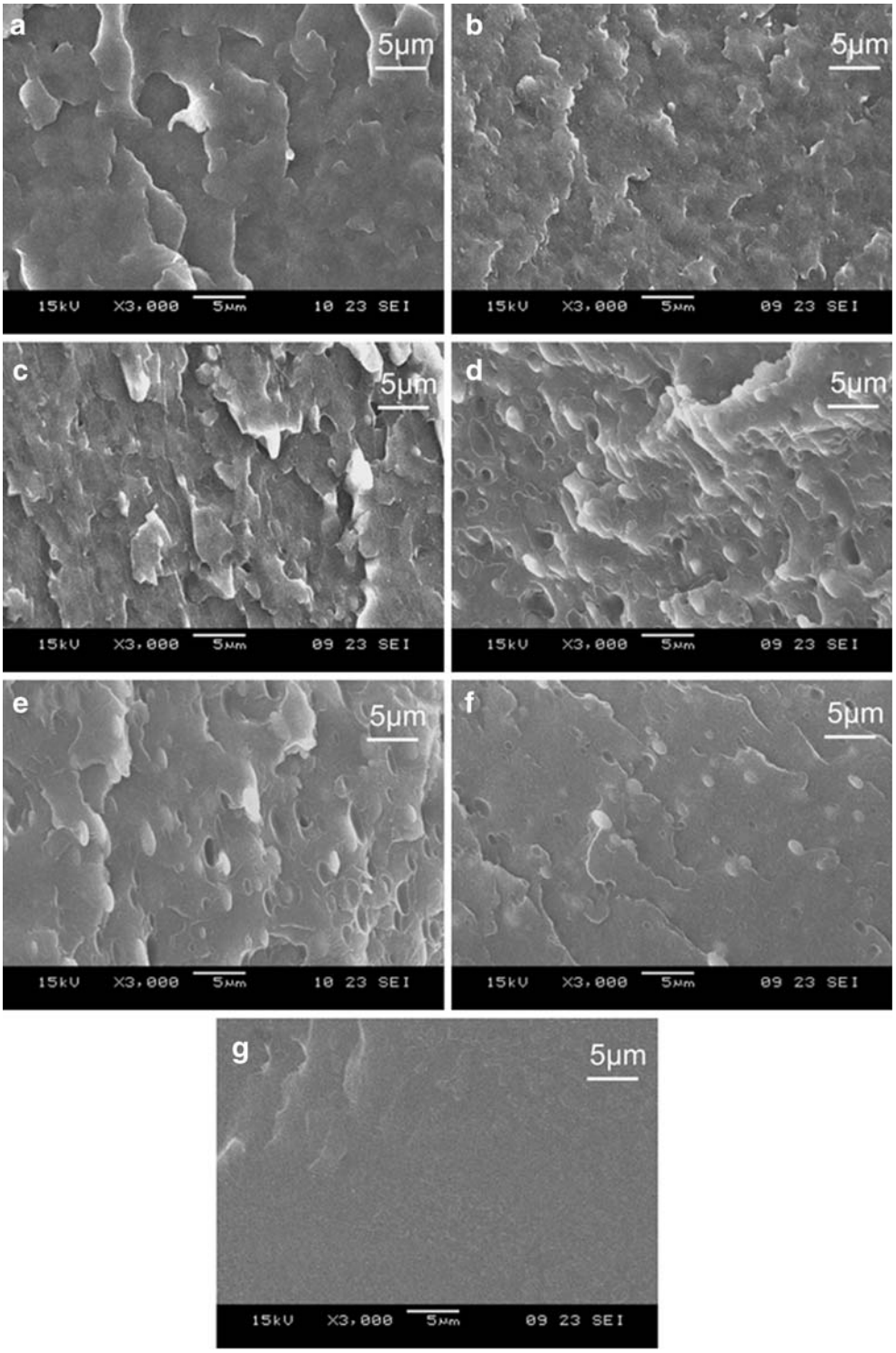

Fig. 1 SEM micrograph of cross section of PVDF/SAN blends with various mass ratios: **a** 100/0, **b** 90/10, **c** 70/30, **d** 50/50, **e** 30/70, **f** 10/90, **g** 0/100

fraction of SAN is half in the blend, only three weak peaks at 2θ=18.05°, 20.27°, and 36.17° are illustrated, and other peaks disappear (Fig. 3d), i.e., the PVDF crystals are decreased more at this composition. In the end, the PVDF crystallization is dramatically hindered by 90 wt.% SAN addition.

Table 1 lists the values of 2θ, interplanar spacing d, according to the three strong peaks observed in the diffractograms of Fig. 3. The lamellar thickness L_{hkl} in the direction perpendicular to the (hkl) crystal plane is calculated by Bragg equation and Scherrer equation [44], as reported in previous works [35, 45]. As shown in

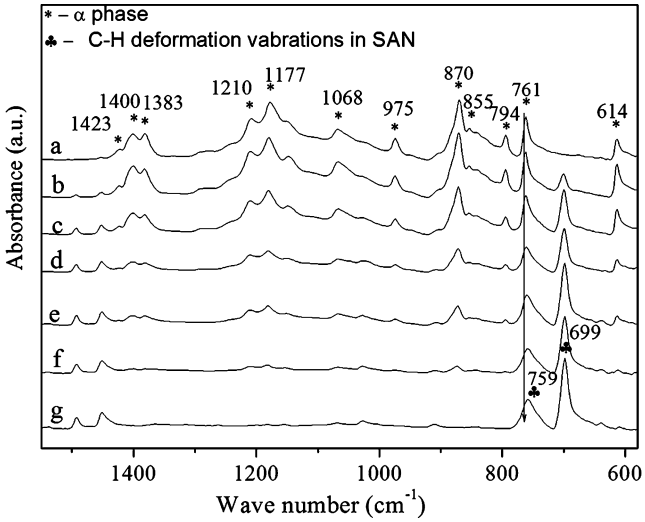

Fig. 2 IR spectra of PVDF/SAN and their blends with various mass ratios: *a* 100/0, *b* 90/10, *c* 70/30, *d* 50/50, *e* 30/70, *f* 10/90, *g* 0/100

Table 1, the value *d* of all planes has nearly no change with the increased SAN addition in the blends, i.e., the lattices parameter of the α phase is not affected by SAN component. However, the values $L_{(100)}$, $L_{(020)}$, and $L_{(110)}$ decrease with the weight fraction of SAN in the melt blend. As demonstrated [35, 45], in the miscible binary blend system such as PVDF/PMMA and PEO/PMMA, the non-crystalline polymer molecules can be sandwiched in inter-lamellar regions, i.e., the value *L* is increased as the non-crystalline polymer composition increased. Herein, the inverse results are obtained. The α phase lamellar thickness of PVDF in the blends is gradually decreased with the increase of SAN addition. Especially for the $L_{(020)}$, as the SAN composition is 30 wt.%, this value cannot be detected. This can be inferred that PVDF/SAN blend is not the completely compatible system. On the other hand, the presence of increased SAN domains causes some kind of perturbation, hindering the lamellar growth of PVDF in the blends.

Thermal properties and crystallinity

Figure 4 shows the DSC melting curves of the melt-crystallized samples. Two melting peaks are observed as the content of PVDF is more than 50 wt.% in the blend. The one possible explanation is the presence of polymorphism of PVDF. In articles, multiphase crystallization of PVDF has been clearly evident in melt-drawn processes [29, 30]. Yang and Thomas observed two endothermic peaks in DSC thermograms and assigned them to melting of α and β phase crystals of PVDF (the lower one for the α-PVDF and the higher for the β-PVDF) [46, 47]. However, as demonstrated by FTIR and WAXD measurements, only one crystalline phase, α phase of PVDF, is present in the melt blends. This evidence implies that the dual-melting peak observed in the melting curves is not due to the polymorphism or the crystal transformation.

The second explanation can be assigned to the melting–recrystallization process [48, 49]. During this process, the melting of the crystallites (small thicknesses) can take place over a temperature interval where subsequent recrystallization is very rapid. Thus, a double-melting peak is observed, and the low-temperature peak represents the melting of the original metastable crystallites, while the high-temperature peak corresponds to the melting of the crystallites perfected during the heating process. However, in this work, the molecular weight of PVDF is high $\left(\overline{\mathrm{M}}\mathrm{w} = 441,000\right)$, and the heating rate is 10 °C/min. As demonstrated by Judovits et al. [50], the high molecular weight and fast heating rate prevent the recrystallization; even when the weight-average molecular weight was 284,000, only a single peak is observed, no matter what the heating rate was. Thus, the recrystallization is very hard to proceed in this work. The further identification of the melting–recrystallization phenomenon will be analyzed in the future work.

The third explanation is related to the lamellar thickness and perfection of PVDF crystals formed during the crystallization from the melt. In Alamo and coworker's work [51], it has been confirmed that the multiple endothermic peaks, which was observed in differential calorimetry as a linear polyethylene went through the melting process, is attributed to a consequence of the distribution of crystallite thickness. Similar result was obtained in poly(4-methyl-1-penten)/dilutes system by Tao's group [52]. Therefore, the two melting peaks observed in this work most possibly belong to the variation

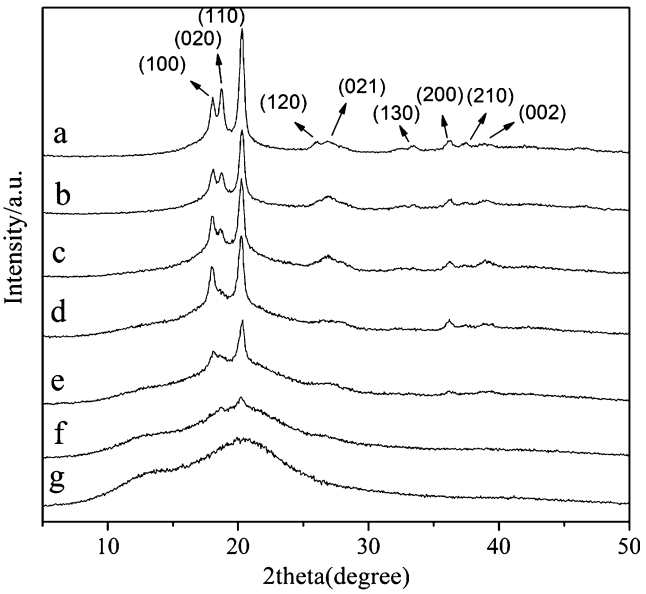

Fig. 3 X-ray diffractograms of PVDF/SAN blends with various mass ratios: *a* 100/0, *b* 90/10, *c* 70/30, *d* 50/50, *e* 30/70, *f* 10/90, *g* 0/100

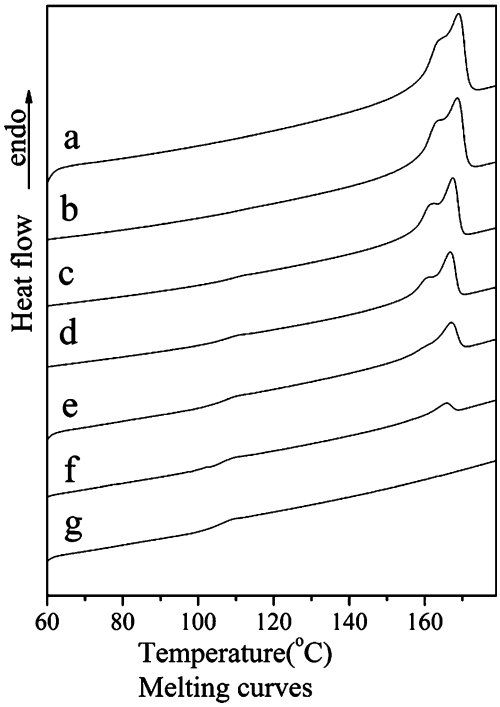

Fig. 4 DSC scans showing the melting traces of PVDF/SAN blends with various mass ratios: *a* 100/0, *b* 90/10, *c* 70/30, *d* 50/50, *e* 30/70, *f* 10/90, *g* 0/100

of the crystallization extent (different crystal size or perfection of crystals), which formed during the sample preparation. The high-temperature peak is related to the melting of more perfect and large-size crystals produced, while the low-temperature peak refers to the imperfect and small-size crystals.

Furthermore, as shown in Fig. 4, a reduction of fusion heat (area of the melt peak, which is proportional to the crystallinity of PVDF) and melting point depression can be observed with an increase of the SAN addition. Especially, for the low-temperature peak, it becomes less intense and moves to the lower one as the SAN composition increased in the blends. As PVDF/SAN=30:70, the low-temperature peak nearly disappears, and only a small melt peak can be observed at PVDF/SAN=10:90. It is suggested that there is an interaction among PVDF and SAN amorphous segments in the blends, which is an indication of the existence of miscibility between these two polymers to some extent [15, 35]. Therefore, the SAN composition in the PVDF blends can affect the crystallization behavior of PVDF obviously. Furthermore, as the SAN content is more than 50 wt.%, the glass transition temperature $T_{g,SAN}$ appears and is nearly the same as that of the neat SAN (Table 2). This suggests that PVDF/SAN blends are not totally miscible, and there occurs stabilization into two phases at the end of the mixing process as SAN≥50 wt.%, as shown in Fig. 1d–f.

Data listed in Table 2, obtained from the melting thermograms (Fig. 4), summarize the influence of the SAN weight fraction on PVDF crystallization in the blends. The onset of melting temperature $\left(T_m^{on}\right)$ of the blends is decreased with an increase of SAN component. Contrary to T_m^{on}, the final melting temperature $\left(T_m^{f}\right)$ has a little decrease. Thus, the increased SAN content leads to the increase in value $\Delta T_m\left(\Delta T_m = T_m^{f} - T_m^{on}\right)$, which means a decrease in the homogeneity of PVDF crystal size. As PVDF crystallizes from the melt in the blends, the different size of PVDF crystals can form, resulting in the multiple melting phenomenon (Fig. 4). The low-temperature peak $\left(T_m^{p1}\right)$, which represents the melting of small-size PVDF crystals, shifts from 164.3 °C to 160.8 °C when 50 wt.% SAN blended with PVDF and disappears as PVDF/SAN=30:70, while the high-temperature peak $\left(T_m^{p2}\right)$, present in each blend sample, represents the melting of the large-size PVDF crystals and decreases a little. This difference implies that the incorporation of SAN dramatically obstructs the formation of the small-size PVDF crystals. Therefore, the heat fusion ΔH obtained from the blends is decreased with an increase of SAN content (Table 2). The observed T_g of SAN in the SAN-rich phase (SAN>50 wt.%) has no obvious change by PVDF segments. It is suggested that the PVDF/SAN blend containing more than 50 wt.% SAN is an immiscible system, as illustrated in the SEM morphologies (Fig. 1d–f).

Table 1 WAXD data of PVDF, SAN, and their blend samples with various mass ratios

PVDF/SAN	*hkl* (100)			*hkl* (020)			*hkl* (110)			*hkl* (021)		
	2θ (°)	*d* (Å)	*L* (Å)	2θ (°)	*d* (Å)	*L* (Å)	2θ (°)	*d* (Å)	*L* (Å)	2θ (°)	*d* (Å)	*L* (Å)
100/0	18.05	4.91	143.9	18.70	4.74	160.2	20.27	4.38	183.1	26.90	3.31	60.6
90/10	18.05	4.91	131.9	18.70	4.74	120.1	20.27	4.38	175.1	26.95	3.31	49.7
70/30	18.05	4.91	119.6	18.65	4.75	–	20.22	4.39	150.0	26.85	3.32	75.7
50/50	18.00	4.92	51.2	–	–	–	20.20	4.39	134.4	–	–	–
30/70	18.03	4.84	61.9	–	–	–	20.26	4.38	83.7	–	–	–
10/90	–	–	–	–	–	–	20.25	4.38	26.8	–	–	–
0/100	–	–	–	–	–	–	–	–	–	–	–	–

– Not observed, θ Bragg angle, *d* the interplanar distance, *L* the thickness of the lamellar crystal (1 Å=10^{-10} m)

Table 2 DSC melting results of PVDF, SAN, and their blend samples with various mass ratios

PVDF/SAN blends	$T_{g,\ SAN}$ (°C)	T_m^{on} (°C)	T_m^{p1} (°C)	T_m^{p2} (°C)	T_m^{f} (°C)	ΔT_m (°C)	ΔH_m (J g^{-1})	X_c (%)
100/0	–	158.1	164.3	169.0	171.7	13.6	40.6	38.9
90/10	–	157.5	163.6	168.6	171.3	13.8	36.7	39.0
70/30	–	156.6	161.7	167.4	169.8	13.2	26.3	36.0
50/50	107.2	155.7	160.8	166.7	169.2	13.5	17.9	34.3
30/70	106.9	153.9	–	167.0	169.9	16.0	10.2	32.5
10/90	106.2	153.1	–	165.6	168.3	15.2	3.0	28.7
0/100	106.5	–	–	–	–	–	–	–

T_m^{on} Onset melting temperature of PVDF, T_m^{p} peak melting temperature of PVDF, T_m^{f} final melting temperature of PVDF, $\Delta T_m = T_m^{f} - T_m^{on}$, ΔH_m melting enthalpy, X_c crystallinity of PVDF

Figure 5 shows the variation of ΔH_m for PVDF crystals with different SAN weight fractions. The value ΔH_m, proportional to the crystallinity of the blends, is normalized for the neat PVDF. The line illustrates the variation in ΔH, if there is no interference of SAN on the crystallization of PVDF in the blends, i.e., PVDF can crystallize in the PVDF/PMMA matrix independently. As observed in Fig. 5, the crystallinity of PVDF is practically unaffected by the incorporation of SAN for values less than 10 wt.%, but at higher additions (>10 wt.% SAN), it is reduced obviously. This indicates that the SAN chains have an influence on the crystallization of PVDF in the blend.

Figure 6 shows the crystallization thermograms of blends with different compositions. In all cases, samples were melted at 180 °C for 10 min and subsequently cooled at a rate of 5 °C/min. The exotherms are observed because of the crystallization of PVDF. It is shown that an increase of the SAN content in the blend reduces the PVDF crystallization temperature progressively, indicating a reduction in the crystallization rate of the PVDF crystals. As SAN composition is higher than 50 wt.%, the crystallization of PVDF presents no evidence. Compared with melting curves in Fig. 4, only one crystallization peak is observed for each sample. This could be attributed to the different crystallization processes for them. The melting curves represent the PVDF crystals formed in the compression molding process (crystallizing at room temperature from the melt). However, the cooling curves reflect the crystallization during cooling process from the melt (at 5 °C/min). In the cooling process, PVDF could crystallize more uniform-size crystals, so only one crystallization peak is observed.

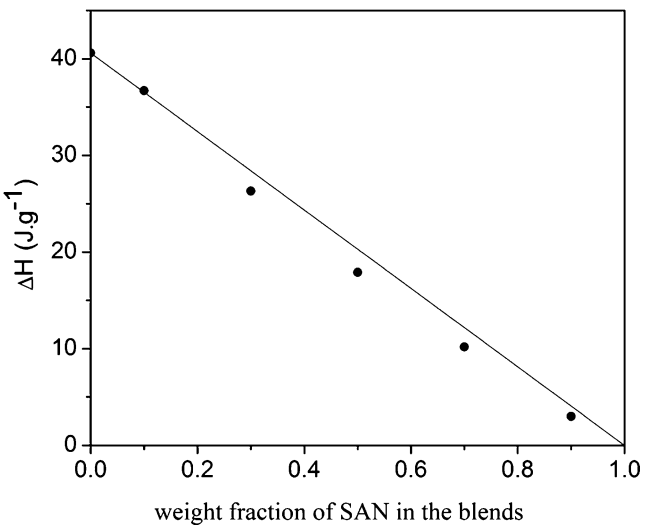

Fig. 5 Area of the endotherm of fusion ΔH of the PVDF crystals against the SAN weight fraction

Table 3 summarizes how the crystallization temperatures and the value of enthalpy of crystallization ΔH_c for PVDF depend upon the weight fraction of SAN observed in Fig. 5. It clearly shows that an increase of SAN weight fraction in the blend retards the crystallization of PVDF progressively, which is similar to the PVDF/PMMA system [32, 35]. The onset crystallization temperature T_c^{on}, peak crystallization temperature T_c^{p}, and final crystallization temperature T_c^{f} are decreased with SAN addition. As the SAN component is more than 50 wt.%, the PVDF crystals fade in the blends when cooling from the melt. However, all the samples with various mass ratios of each component in the blends, crystallizing from the melt at the room temperature, have the melting traces (Fig. 4). It is suggested that the crystallization of PVDF from the melt at the room

Table 3 DSC crystallization results of PVDF, SAN, and their binary blends

PVDF/SAN blends	T_c^{on} (°C)	T_c^{p} (°C)	T_c^{f} (°C)	ΔT_c (°C)	ΔH_c (J g^{-1})	$t_{1/2}$ (min)
100/0	147.9	144.6	141.9	6.0	41.0	0.47
90/10	145.3	141.2	138.4	6.9	39.9	0.54
70/30	144.0	139.8	137.2	6.8	28.3	0.54
50/50	142.1	138.1	134.7	7.4	17.0	0.61
30/70	–	–	–	–	–	–
10/90	–	–	–	–	–	–
0/100	–	–	–	–	–	–

T_c^{on} Onset crystallization temperature of PVDF, T_c^{p} peak crystallization temperature of PVDF, T_c^{f} final crystallization temperature of PVDF, $\Delta T_c = T_c^{on} - T_c^{f}$, ΔH_c crystallization enthalpy of PVDF

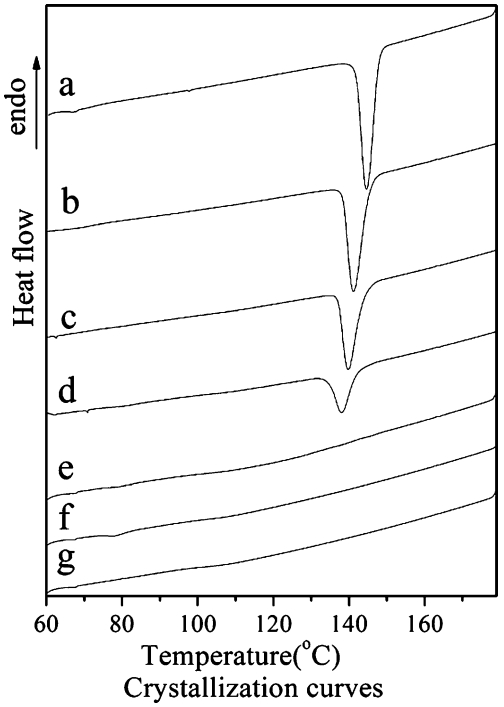

Fig. 6 DSC scans showing the crystallization traces of PVDF/SAN blends with various mass ratios: *a* 100/0, *b* 90/10, *c* 70/30, *d* 50/50, *e* 30/70, *f* 10/90, *g* 0/100

temperature is quite easy in comparison with the one at the cooling rate of 5 °C/min. Besides, the value ΔT_c expands with the increased SAN addition. This means that the crystallization rate of PVDF in the blends from the melt is decreased. As estimated, the crystallization half time $t_{1/2}$ is increased as the SAN content increased in the blends. It has been reported that the smaller the $t_{1/2}$, the more quickly the crystallization processed is [53]. Therefore, the addition of SAN can reduce the rate of crystallization of PVDF. This also confirms that the more SAN content in the blend, the more influence on the PVDF crystallization performs.

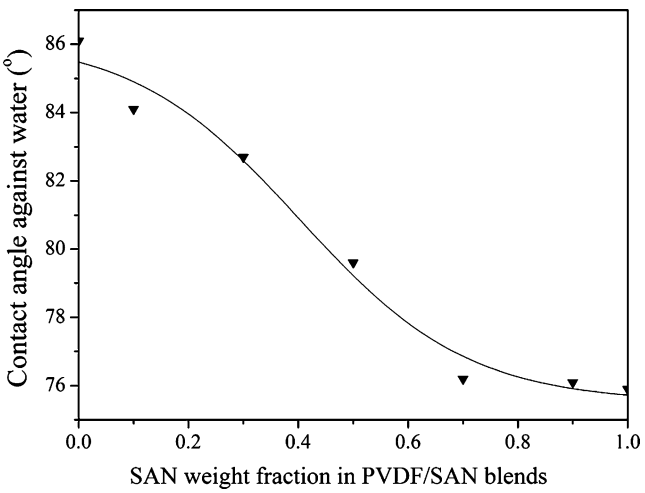

Fig. 7 The contact angle against water as a function of SAN contents in the blends

Table 4 Contact angles of distilled water and diiodomethane, solid surface tensions γ_s, and its components γ_s^d, γ_s^p

Surfaces of PVDF/SAN blends	Contact angle (°)		Surface tensions (mJ/m^2)		
	Distilled water	Diiodomethane	γ_s	γ_s^d	γ_s^p
100/0	86.1	37.4	41.23	38.63	2.60
90/10	84.1	28.6	45.09	42.55	2.54
70/30	82.7	28.4	45.32	42.37	2.95
50/50	79.6	36.3	43.60	38.80	4.80
30/70	76.2	25.2	47.52	42.36	5.16
10/90	76.7	26.7	46.95	41.87	5.08
0/100	75.9	24.2	47.87	42.67	5.20

Contact angle test

Contact angles are the characteristic constants of liquid/solid systems and provide valuable information on the surface energies of solids. Usually, the lower the contact angle against water, the more hydrophilic the sample is [35, 54]. In Fig. 7, the contact angles against water decrease dramatically as the SAN weight fraction increased until 70 wt.%, and above this point, it decreases slightly. This indicates that the SAN addition increases the hydrophilicity of the PVDF. It can be seen that the region ranging from about 30 to 70 wt.% SAN addition performs steeper decreasing of the contact angle. Hence, an obvious hydrophobic–hydrophilic transition is approximately observed in this section. As the SAN content is less than 30 wt.%, the surface of the blend consists primarily of the crystalline PVDF and PVDF may besiege the SAN phase (Fig. 1a,b). In this case, the surface hydrophilicity rises slightly. In contrast, as the SAN content is greater than 70 wt.%, the surface of the blend consists

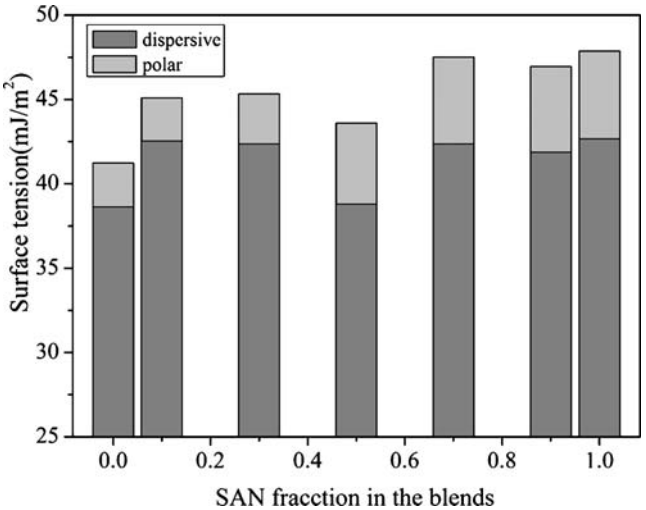

Fig. 8 The surface tension including dispersive and polar component as a function of SAN content in the blends

chiefly of the amorphous PVDF/SAN matrix and the occurrence of besieging the PVDF by the rich SAN phase (Fig. 1e,f). In this region, the value of the contact angle against water decreases a little or even close to that of the neat SAN surface.

In the present study, the PVDF/SAN blends with various mass ratios of each component were tested with two liquids. Subsequently, the total surface tension γ_s, which consists of the two components of dispersive part γ_s^d and polar part γ_s^p, corresponds to what was determined in our previous work [35]. The results are given in Table 4. The contact angle against water decreases from 86.1° to 75.9° and against diiodomethane from 37.4° to 24.2°. It implies that the hydrophobic character of PVDF is reduced by addition of SAN to some extent, whereas the contact angle against diiodomethane of the sample with 50 wt.% SAN addition is close to the value of neat PVDF. This fluctuation may be attributed to the obvious existence of inhomogeneity of the blend owing to the phase inversion reasonably when 50 wt.% SAN was added (Fig. 1d).

In SAN, the nitrile group (–CN) renders this material the hydrophilic property [23]. As calculated by the Owens–Wendt approach [37], the total surface tension γ_s of SAN (47.87 mJ/m^2) is higher than PVDF (41.23 mJ/m^2), especially for the polar component γ_s^p (Table 4). Thus, the surface tension of PVDF can be improved by blending with SAN. In Fig. 8, it can be seen that the surface tension is increased with an increase of SAN addition, especially for the polar part. When 50 wt.% SAN blended with PVDF, the polar part γ_s^p is nearly close to the neat SAN sample owing to SAN besieging the PVDF phase. In this case, the loss hydrophobicity becomes apparent with the participation of SAN into the hydrophobically predominated surface. Additionally, the surface tension of the blend containing 50 wt.% SAN is the lowest in the polyblend samples. This may be attributed to the worse miscibility, and the phase inversion (from PVDF- to SAN-rich phase) occurs (Fig. 1d).

Conclusion

Summarizing the results presented above, it is clearly confirmed by FTIR and WAXD that the PVDF component presented only α phase in the PVDF/SAN blends, which were prepared from melting states. Melting point depression indicated that the SAN amorphous segments had an effect on the crystallization of PVDF. During the DSC heating process, two melting peaks were observed. The low-temperature endotherm was due to the melting of the small-size PVDF crystals, which shifted to lower temperature with an increase of SAN content. However the high-temperature peak, which was assigned to the large-size PVDF crystals, had little decrease. In the blends, the growth of PVDF lamellar was obstructed by SAN segments in the blends, resulting in a decrease of lamellar thickness and the crystallinity as SAN content increased. SEM showed a good connection between PVDF and SAN phase as SAN< 50 wt.%. In contrast, the crystalline PVDF particle clearly disperses in the SAN and PVDF amorphous matrix, and the size of crystalline PVDF particle decreases with the further increase of SAN content in SAN, which exceeded 50 wt.%. Therefore, the PVDF/SAN blend system was partially miscible as the SAN content was lower than 50 wt.%.

On the other hand, the hydrophilicity of PVDF can be improved by blending with SAN. Through contact angles test and calculation of surface tension of the blend surface, the total surface tension increased with SAN addition mainly because of the increased of the polar component contribution. As the SAN content reached 70 wt.%, the stable hydrophilicity was obtained because SAN besieged the PVDF phase.

Acknowledgment Financial support from the Key Project of BMSTC (D0406003040191) is gratefully acknowledged.

References

1. Seiler DA (1997) In: Scheirs J (ed) Modern fluoropolymers. Wiley, Chichester, p 487
2. Nunes SP, Peinemann KV (2001) In: Nunes SP, Peinemann KV (eds) Membrane technology in the chemical industry. Wiley, Weinheim, p 12
3. Gu M, Zhang J, Wang X, Tao H (2006) Desalination 192:160
4. Gu M, Zhang J, Wang X, Ma W (2006) J Appl Polym Sci 102:3714
5. Buonomenna M, Macchi P, Davoli M, Drioli E (2007) Eur Polym J 43:1557
6. Chen YW, Liu DM, Zhang N (2005) Surf Rev Lett 12:709
7. Marmey P, Porte MC, Baquey C (2003) Nucl Instrum Methods Phys Res, Sect B 208:429
8. Hietala S, Skou E, Sundholm F (1999) Polymer 40:5567
9. Duca M, Plosceanu CL, Pop T (1998) Polym Degrad and Stab 61:65
10. Brondino C, Boutevin B, Parisi JP, Schrynemackers J (1999) J Appl Polym Sci 72:611
11. Zhai GQ, Toh SC, Tan WL, Kang ET, Neoh KG (2003) Langmuir 19:7030
12. Liu X, Neoh KG, Kang ET (2003) Macromolecules 36:8361
13. Ying L, Kang ET, Neoh KG (2002) Langmuir 18:6416
14. Linares A, Acosta JL (1998) J Appl Polym Sci 67:997
15. Nishi T, Wang TT (1975) Macromolecules 8:909
16. Sasaki H, Bala PK, Yoshida H, Ito E (1995) Polymer 36:4805
17. Roerdink E, Challa G (1978) Polymer 19:173
18. Nunes SP, Peinemann KV (1992) J Membr Sci 73:25
19. Ochoa NA, Masuelli M, Marchese J (2003) J Membr Sci 226:203
20. Chen NP, Hong L (2002) Polymer 43:1429
21. Hester JF, Banerjee P, Mayes AM (1999) Macromolecules 32:1643
22. Hester JF, Mayes AM (2002) J Membr Sci 202:119
23. Yang MC, Liu TY (2003) J Membr Sci 226:119
24. Yin X, Cheng H, Wang X, Yao Y (1998) J Membr Sci 146:179
25. Moussaif N, Jerome R (1999) Polymer 40:3919

26. Liu TY, Lin WC, Huang LY, Chen SY, Yang MC (2005) Polym Adv Technol 16:413
27. Lovinger AJ, Keith HD (1979) Macromolecules 12:919
28. Lovinger AJ (1980) J Polym Sci, Polym Phys Ed 18:793
29. Gregorio Jr R, Cestari M (1994) J Polym Sci, Part B: Polym Phys 32:859
30. Gregorio Jr R (2006) J Appl Polym Sci 100:3272
31. Zhou XX, Cakmak M (2007) J Macromol Sci, Part B: Phys 46:667
32. Gregorio R Jr, Nociti NCPS (1995) J Phys D: Appl Phys 28:432
33. Ma W, Zhang J, Wang X (2007) Appl Surf Sci 254:2947
34. Ma W, Zhang J, Wang X (2007) J Mater Sci 43:398
35. Ma W, Zhang J, Wang X, Wang S (2007) Appl Surf Sci 253:8377
36. Long Y, Shanks RA, Stachurski ZH (1995) Polymer 20:651
37. Owens DK, Wendt RC (1969) J Appl Polym Sci 13:1741
38. Spelt JK (1990) Colloids Surf 43:389
39. Grulke EA (1999) In: Brandrup J, Immergut EH (eds) Polymer handbook. Wiley, USA, p VII 675
40. Kobayashi M, Tashiro K, Tadokoro H (1975) Macromolecules 8:158
41. Sun YP, Lawson GE, Bunker CE, Johnson RA, Ma B, Farmer C, Riggs JE, Kitaygorodskiy A (1996) Macromolecules 29:8441
42. Davis GT, McKinney JE, Broadhurst MG, Roth SC (1978) J Appl Phys 49:4998
43. Hodge RM, Edward GH, Simon GP (1996) Polymer 3:1371
44. Suryanarayana C, Grant NM (1998) X-ray diffraction: a practical approach. Plenum, New York
45. Martuscelli E, Canetti M, Vicini L, Seves A (1982) Polymer 23:331
46. Yang DC, Thomas EL (1984) J Mater Sci Lett 3:929
47. Yang DC, Thomas EL (1987) J Mater Sci Lett 6:593
48. Nakawa K, Ishida Y (1973) J Polym Sci, Polym Phys Ed 11:2153
49. Marega C, Marigo A (2003) Eur Polym J 39:1713
50. Judovits L, Menczel JD, Leray AG (1998) J Therm Anal Calorim 54:605
51. Alamo R, Mandelkern L (1986) J Polym Sci, Part B: Polym Phys 24:2087
52. Tao H, Zhang J, Wang X, Gao J (2007) J Polym Sci, Part B: Polym Phys 45:153
53. Wang J, Dou Q, Wu S, Chen X (2007) Polym Eng Sci 47:889
54. Huang C, Zhang L (2004) J Appl Polym Sci 92:1